


 Cite this: *RSC Adv.*, 2023, 13, 31881

# The effect of $\text{MnCO}_3$ on the gain coefficient for the ${}^4\text{I}_{13/2} \rightarrow {}^4\text{I}_{15/2}$ transition of $\text{Er}^{3+}$ ions and near-infrared emission bandwidth flatness of $\text{Er}^{3+}/\text{Tm}^{3+}/\text{Yb}^{3+}$ co-doped barium zinc silicate glasses†

 Ho Kim Dan,<sup>a,b</sup> Nguyen Dinh Trung,<sup>c,d</sup> Nguyen Minh Tam,<sup>e</sup> L. T. Ha,<sup>b,\*f</sup> Nguyen Le Thai,<sup>g</sup> Tran Dang Thanh,<sup>h</sup> Dacheng Zhou<sup>i</sup> and Jianbei Qiu<sup>i</sup>

The roles of  $\text{Mn}^{2+}$  ions in the  $\text{MnCO}_3$  compound, leading to the formation of an  $\text{Mn}^{2+}-\text{Yb}^{3+}$  dimer and affecting the gain coefficient for the  ${}^4\text{I}_{13/2} \rightarrow {}^4\text{I}_{15/2}$  transition of  $\text{Er}^{3+}$  ions and near-infrared (NIR) emission bandwidth flatness of  $\text{Er}^{3+}/\text{Tm}^{3+}/\text{Yb}^{3+}$  co-doped in  $\text{SiO}_2-\text{ZnO}-\text{BaO}$  (SZB) barium zinc silicate glasses, were investigated in this work. The composition of all elements from the original raw materials that exist in the host glasses was determined using energy-dispersive X-ray spectroscopy (EDS). Under the excitation of a 980 nm laser diode (LD), the NIR emission of  $\text{Er}^{3+}/\text{Tm}^{3+}/\text{Yb}^{3+}$ -co-doped SZB glasses produced a bandwidth of about 430 nm covering the O, E, and C bands. The effects of  $\text{Mn}^{2+}$  ions and the  $\text{Mn}^{2+}-\text{Yb}^{3+}$  dimer on the gain coefficient for the  ${}^4\text{I}_{13/2} \rightarrow {}^4\text{I}_{15/2}$  transition of  $\text{Er}^{3+}$  ions and bandwidth flatness of NIR emission of  $\text{Er}^{3+}/\text{Tm}^{3+}$ -co-doped and  $\text{Er}^{3+}/\text{Tm}^{3+}/\text{Yb}^{3+}$ -co-doped SZB glasses were also assigned. The optimal molar concentration of  $\text{Mn}^{2+}$  ions was determined such that the NIR bandwidth flatness of  $\text{Er}^{3+}/\text{Tm}^{3+}/\text{Yb}^{3+}$ -co-doped SZB glasses was the flattest. In addition, the role of  $\text{Mn}^{2+}$  ions in reducing the gain coefficient for the  ${}^4\text{I}_{13/2} \rightarrow {}^4\text{I}_{15/2}$  transition of  $\text{Er}^{3+}$  ions was also calculated and discussed.

 Received 18th September 2023  
 Accepted 17th October 2023

DOI: 10.1039/d3ra06348h

[rsc.li/rsc-advances](https://rsc.li/rsc-advances)

## 1. Introduction

The near-infrared (NIR) emission spectra of rare earth ions (REIs), such as  $\text{Pr}^{3+}$ ,  $\text{Er}^{3+}$ ,  $\text{Tm}^{3+}$ , and  $\text{Ho}^{3+}$  ions, in the wavelength range from  $\sim 1200$  to  $2000$  nm with the coverage of long-band (L-band), ultra-band (U-band), and (L + U)-bands have been of interest to researchers due to their expected applications in optical amplifiers and fibre lasers.<sup>1–3</sup> The NIR emission spectra of the  $\text{Er}^{3+}$ -doped peak at about 1545 nm and of the

$\text{Tm}^{3+}$ -doped peak at about 1769 nm, corresponding to  ${}^4\text{I}_{13/2} \rightarrow {}^4\text{I}_{15/2}$  (ref. 4) and  ${}^3\text{F}_4 \rightarrow {}^3\text{H}_6$  transitions, respectively, have been widely investigated because of their typical applications in an erbium-doped fiber amplifier (EDFA)<sup>5,6</sup> and a thulium-doped fiber amplifier (TDFA).<sup>7</sup> While  $\text{Er}^{3+}$  ions can be directly excited by commercial wavelengths of both 808 nm LD and 980 nm LD,<sup>1,5,6,8</sup>  $\text{Tm}^{3+}$  ions can only be directly excited by the wavelength of an 808 nm LD but not by a 980 nm LD.<sup>9,10</sup> Therefore, for the NIR emission spectra of  $\text{Tm}^{3+}$ -doped and  $\text{Er}^{3+}/\text{Tm}^{3+}$ -co-doped glasses using a commercial wavelength 980 nm LD for excitation,  $\text{Yb}^{3+}$  ions are often introduced as a sensitizer or for a cooperative energy transfer (CET) process through dimers/trimers such as a  $\text{Yb}^{3+}-\text{Yb}^{3+}$  dimer,<sup>11</sup>  $\text{Cr}^{3+}-\text{Yb}^{3+}$  dimer,<sup>12</sup>  $\text{Mn}^{2+}-\text{Yb}^{3+}$  dimer,<sup>13,14</sup> or  $\text{Mn}^{2+}-\text{Mn}^{2+}-\text{Yb}^{3+}$  trimer<sup>4,15</sup> for direct excitation by the commercial wavelength of a 980 nm LD.<sup>16</sup> Among the dimers, the  $\text{Mn}^{2+}-\text{Yb}^{3+}$  dimer formed by transition metal ions  $\text{Mn}^{2+}$  and  $\text{Yb}^{3+}$  ions is commonly used for the CET process of NIR emission spectra of  $\text{Tm}^{3+}$  doped or  $\text{Er}^{3+}/\text{Tm}^{3+}$  co-doped in host glasses.<sup>13,14,17</sup> In addition to expanding the NIR spectral bandwidth for REIs, recent studies have also focused on investigating and finding solutions to flatten the NIR spectral bandwidth of these REIs to optimize the obtained NIR spectral bandwidth for optical applications.<sup>18–22</sup> In our previous studies,<sup>23,24</sup> we investigated, calculated, and reported solutions to widen the bandwidth as well as to enhance the near-infrared bandwidth flatness of  $\text{Tm}^{3+}$ -doped,  $\text{Ho}^{3+}$ -doped,  $\text{Tm}^{3+}/\text{Ho}^{3+}$ -co-

<sup>a</sup>Optical Materials Research Group, Science and Technology Advanced Institute, Van Lang University, Ho Chi Minh City, Vietnam. E-mail: hokimdan@vlu.edu.vn

<sup>b</sup>Faculty of Applied Technology, School of Technology, Van Lang University, Ho Chi Minh City, Vietnam

<sup>c</sup>Center for Analysis and Testing, Dalat University, Lam Dong, Vietnam

<sup>d</sup>Faculty of Chemistry and Environment, Dalat University, Lam Dong, Vietnam

<sup>e</sup>Faculty of Basic Sciences, University of Phan Thiet, 225 Nguyen Thong, Phan Thiet City, Binh Thuan, Vietnam

<sup>f</sup>Institute of Science and Technology, TNU-University of Sciences, Thai Nguyen, 250000, Vietnam. E-mail: halt@tnus.edu.vn

<sup>g</sup>Faculty of Engineering and Technology, Nguyen Tat Thanh University, Ho Chi Minh City, Vietnam

<sup>h</sup>Institute of Materials Science, Vietnam Academy of Science and Technology (VAST), 18 Hoang Quoc Viet, Hanoi, Vietnam

<sup>i</sup>Key Laboratory of Advanced Materials of Yunnan Province, Kunming University of Science and Technology, Kunming, 650093, China

 † Electronic supplementary information (ESI) available. See DOI: <https://doi.org/10.1039/d3ra06348h>


doped, and Ho<sup>3+</sup>/Tm<sup>3+</sup>/Yb<sup>3+</sup>-co-doped glasses.<sup>19,23</sup> The obtained results indicated that the NIR bandwidth flatness of Tm<sup>3+</sup>-doped, Ho<sup>3+</sup>-doped, Tm<sup>3+</sup>/Ho<sup>3+</sup>-co-doped, and Ho<sup>3+</sup>/Tm<sup>3+</sup>/Yb<sup>3+</sup>-co-doped glasses was significantly improved by the presence of Mn<sup>2+</sup> ions and an Mn<sup>2+</sup>-Yb<sup>3+</sup> dimer in the host glasses.<sup>13,14,23</sup>

Following the positive results described above, in this work, we continue to examine and report the effects of Mn<sup>2+</sup> ions and Mn<sup>2+</sup>-Yb<sup>3+</sup> dimers on the gain coefficient for the <sup>4</sup>I<sub>13/2</sub> → <sup>4</sup>I<sub>15/2</sub> transition of Er<sup>3+</sup> ions and NIR emission bandwidth flatness of Er<sup>3+</sup>/Tm<sup>3+</sup>/Yb<sup>3+</sup>-co-doped barium zinc silicate glasses with the aim of clarifying the roles of Mn<sup>2+</sup> ions in the MnCO<sub>3</sub> compound in the formation of an Mn<sup>2+</sup>-Yb<sup>3+</sup> dimer. Remarkably, we have attempted to determine not only the optimal BFN\_NIR emission of Er<sup>3+</sup>/Tm<sup>3+</sup>/Yb<sup>3+</sup>-co-doped SZB glasses but also the optimal molar concentration of Mn<sup>2+</sup> ions in the MnCO<sub>3</sub> compound such that the BFN\_NIR emission of Er<sup>3+</sup>/Tm<sup>3+</sup>/Yb<sup>3+</sup>-co-doped SZB glasses is a maximum. In addition, the role of Mn<sup>2+</sup> ions in the MnCO<sub>3</sub> compound in reducing the gain coefficient for the <sup>4</sup>I<sub>13/2</sub> → <sup>4</sup>I<sub>15/2</sub> transition of Er<sup>3+</sup> ions was also examined. The obtained results are able to guide the selection of more optimal materials for EDFA and TDFA optical amplifiers.

## 2. Experimental details

### 2.1. Materials

In this experiment, the glass materials are fabricated by the conventional melting method. All the raw materials consisting of SiO<sub>2</sub>, ZnO, BaO, TiO<sub>2</sub>, MnCO<sub>3</sub>, Er<sub>2</sub>O<sub>3</sub>, Tm<sub>2</sub>O<sub>3</sub>, and Yb<sub>2</sub>O<sub>3</sub> used in this study are laboratory reagents with high purity (99.99%).

The abbreviations, chemical compositions, and detailed molar ratios are listed in Table 1.

### 2.2. Experimental methods

Approximately 12 g of the mixtures of raw materials were weighed for each glass sample using an electronic analytical balance. After being finely ground using an onyx mortar and pestle, these mixtures were compressed into a platinum crucible and were then heated in a German-manufactured Nabertherm electric furnace at 1580 °C for a continuous period of 50 minutes, under an air atmosphere.<sup>23</sup> In the process of fabrication of the host glass and the glass doped with rare earth elements, the raw material mixtures after fine grinding are often heated at a temperature that is equal to or greater than the glass transition temperature of the raw materials, (abbreviated  $T_g$ ). This temperature  $T_g$  is related to the melting point temperature of the materials ( $T_m$ ) through the expression  $T_g = \frac{2}{3}T_m$ .<sup>24,25</sup> In the experiment in this study, the SiO<sub>2</sub>, ZnO, TiO<sub>2</sub>, BaO, Er<sub>2</sub>O<sub>3</sub>, Tm<sub>2</sub>O<sub>3</sub>, and Yb<sub>2</sub>O<sub>3</sub> raw material mixtures have melting points greater than 1580 °C. However, we chose the material melting temperature of 1580 °C<sup>23</sup> at which these material mixtures are melted enough to form glasses.<sup>23,24</sup> In the next step, the melted mixtures were poured into a mold and quenched on the surface of a stainless steel plate to form the raw glass. To increase the mechanical strength and remove thermal strain from the raw glass, all raw glass samples were annealed at ~500 °C for a continuous period of 12 hours.<sup>17,19,23,26</sup> The glass samples used for optical measurements were cut to a size of ~10 mm × 10 mm × 2 mm. The edges and surfaces of these glass samples were then thoroughly polished.

**Table 1** Detailed chemical composition and concentration ratios of SiO<sub>2</sub>-ZnO-BaO-TiO<sub>2</sub>-Er<sub>2</sub>O<sub>3</sub>-Tm<sub>2</sub>O<sub>3</sub>-MnCO<sub>3</sub>-Yb<sub>2</sub>O<sub>3</sub> barium zinc silicate glasses

Name of glass sample	Details of composition and molar concentration (in mol%)							
	SiO <sub>2</sub>	ZnO	BaO	TiO <sub>2</sub>	Er <sub>2</sub> O <sub>3</sub>	Tm <sub>2</sub> O <sub>3</sub>	MnCO <sub>3</sub>	Yb <sub>2</sub> O <sub>3</sub>
SZB-2Mn2Yb	45	26	17	8	0	0	2	2
SZB-0.5Er	45	26	20.5	8	0.5	0	0	0
SZB-1Tm	45	26	20	8	0	1	0	0
SZB-0.5Er2Yb	45	26	18.5	8	0.5	0	0	2
SZB-0.5Er2Yb2Mn	45	26	16.5	8	0.5	0	2	2
SZB-0.5Er2Yb2.5Mn	45	26	16	8	0.5	0	2.5	2
SZB-0.5Er2Yb3Mn	45	26	15.5	8	0.5	0	3	2
SZB-0.5Er2Yb3.5Mn	45	26	15	8	0.5	0	3.5	2
SZB-0.5Er2Yb4Mn	45	26	14.5	8	0.5	0	4	2
SZB-1Tm2Yb	45	26	18	8	0	1	0	2
SZB-1Tm2Yb2Mn	45	26	16	8	0	1	2	2
SZB-1Tm2Yb2.5Mn	45	26	15.5	8	0	1	2.5	2
SZB-1Tm2Yb3Mn	45	26	15	8	0	1	3	2
SZB-1Tm2Yb3.5Mn	45	26	14.5	8	0	1	3.5	2
SZB-1Tm2Yb4Mn	45	26	14	8	0	1	4	2
SZB-0.5Er1Tm2Yb	45	26	17.5	8	0.5	1	0	2
SZB-0.5Er21TmYb2Mn	45	26	15.5	8	0.5	1	2	2
SZB-0.5Er1Tm2Yb2.5Mn	45	26	15	8	0.5	1	2.5	2
SZB-0.5Er1Tm2Yb3Mn	45	26	14.5	8	0.5	1	3	2
SZB-0.5Er1Tm2Yb3.5Mn	45	26	14	8	0.5	1	3.5	2
SZB-0.5Er1Tm2Yb4Mn	45	26	13.5	8	0.5	1	4	2



The EDS spectrum was carried out using field emission scanning electron microscopy (FE-SEM), with a Jeol JSM-6510LV. Optical transmittance spectra of the glass within the wavelength range of 350 to 2000 nm were carried out using a Hitachi U-4100 UV/VIS/NIR spectrophotometer. NIR emission spectra of the glass within the wavelength range of 1300 to 2100 nm were measured using a Zolix SBP300 spectrophotometer with an InGaAs detector under excitation by a 980 nm LD. Optical transmittance and NIR emission spectra measurements as well as EDS analysis of the glass samples were performed at ambient temperature.<sup>17,19</sup>

### 3. Results and discussion

#### 3.1. EDS analysis

To determine whether the elements in the original raw material still exist in the glass materials after fabrication, we conducted an EDS analysis for the SZB-0.5Er1Tm2Yb2Mn glass sample, and the analyzed results within the energy range from 0 to 10 keV are plotted in Fig. 1. The energy levels of each element are listed in detail in Table 2. The obtained results of the EDS spectrum analysis of the SZB-0.5Er1Tm2Yb2Mn glass sample confirmed that the C, Ti, O, Ba, Zn, Si, Mn, Tm, Er, and Yb elements were still present in the  $\text{SiO}_2\text{-ZnO-BaO-TiO}_2\text{-Er}_2\text{O}_3\text{-Tm}_2\text{O}_3\text{-MnCO}_3\text{-Yb}_2\text{O}_3$  glass matrix.<sup>27,28</sup> It should be noted that

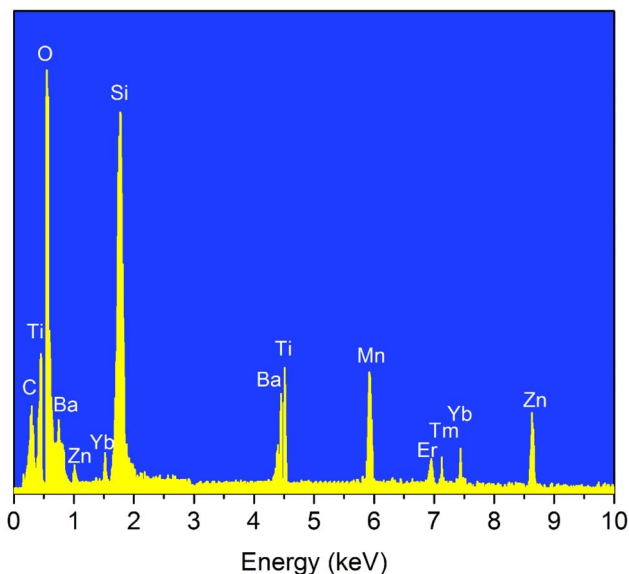


Fig. 1 EDS spectral analysis of the SZB-0.5Er1Tm2Yb2Mn glass sample.

Table 2 Details of the energy levels of the elements in the EDS spectral analysis

Energy	Element									
	C	Ti	O	Ba	Zn	Si	Mn	Er	Tm	Yb
$L_{\alpha}$ (keV)	0.278	0.452	0.526	0.971	1.012	1.741	0.638	1.405	7.179	1.521
$K_{\alpha}$ (keV)		4.509		4.466	8.629		5.895	6.946		7.415

the Mn element has many different valence states, including +2, +3, +4, +5, +6, and +7 valences. When the  $\text{MnCO}_3$  compound is introduced into the host glasses, the Mn element exists almost exclusively in the Mn 2p1 and Mn 2p3 valence states and this was investigated through XPS analysis and reported in a previous study.<sup>17</sup> Following the results achieved on the behavior of the  $\text{MnCO}_3$  compound doped into barium zinc silicate glasses, the goal of this work is mainly to focus on investigating the role of  $\text{Mn}^{2+}$  ions in the  $\text{MnCO}_3$  compound for combining to form an  $\text{Mn}^{2+}\text{-Yb}^{3+}$  dimer and transferring energy to  $\text{Er}^{3+}$  and  $\text{Tm}^{3+}$  ions to enhance the NIR emission intensity of  $\text{Er}^{3+}/\text{Tm}^{3+}/\text{Yb}^{3+}$ -co-doped barium zinc silicate glasses under 980 nm LD excitation.

#### 3.2. Optical transmittance spectra

In Fig. 2(A), optical transmittance spectra of the SZB-0.5Er, SZB-0.5Er2Yb2Mn, SZB-1Tm, and SZB-1Tm2Yb2Mn glass samples are shown in curves (a), (b), (c) and (d), respectively. Curve (a) shows the optical transmittance spectra of the  $\text{Er}^{3+}$ -doped sample in which seven optical transmittance bands can be observed corresponding to the  $^4\text{I}_{15/2} \rightarrow ^4\text{G}_{11/2}$ ,  $^4\text{F}_{7/2}$ ,  $^2\text{H}_{11/2}$ ,  $^4\text{S}_{3/2}$ ,  $^4\text{F}_{9/2}$ ,  $^4\text{I}_{11/2}$  and  $^4\text{I}_{13/2}$  transitions of  $\text{Er}^{3+}$  ions.<sup>29,30</sup> Curve (b) shows the optical transmittance spectrum of the  $\text{Er}^{3+}/\text{Yb}^{3+}/\text{Mn}^{2+}$ -co-doped sample in which nine optical transmittance bands can be observed, among which, one corresponds to the  $^6\text{A}_{1g} \rightarrow ^4\text{T}_{1g}$  transition of  $\text{Mn}^{2+}$  ions,<sup>13,14,17</sup> one corresponds to the  $^2\text{F}_{7/2} \rightarrow ^2\text{F}_{5/2}$  transition of  $\text{Yb}^{3+}$  ions,<sup>27,28</sup> and the remaining seven correspond to the  $^4\text{I}_{15/2} \rightarrow ^4\text{G}_{11/2}$ ,  $^4\text{F}_{7/2}$ ,  $^2\text{H}_{11/2}$ ,  $^4\text{S}_{3/2}$ ,  $^4\text{F}_{9/2}$ ,  $^4\text{I}_{11/2}$  and  $^4\text{I}_{13/2}$  transitions of  $\text{Er}^{3+}$  ions.<sup>30,31</sup> Curve (c) shows the optical transmittance spectra of the  $\text{Tm}^{3+}$ -doped in SZB-1Tm glass sample in which five optical transmittance bands can be observed corresponding to the  $^3\text{H}_6 \rightarrow ^1\text{G}_4$ ,  $^3\text{F}_{2,3}$ ,  $^3\text{H}_4$ ,  $^3\text{H}_5$ , and  $^3\text{F}_4$  transitions of  $\text{Tm}^{3+}$  ions. Curve (d) shows the optical transmittance spectra of the  $\text{Tm}^{3+}/\text{Yb}^{3+}/\text{Mn}^{2+}$  co-doped in SZB-1Tm2Yb2Mn glass sample in which seven optical transmittance bands can be observed, among which, one corresponds to the  $^6\text{A}_{1g} \rightarrow ^4\text{T}_{1g}$  transition of  $\text{Mn}^{2+}$  ions,<sup>13,14,17</sup> one corresponds to the  $^2\text{F}_{7/2} \rightarrow ^2\text{F}_{5/2}$  transition of  $\text{Yb}^{3+}$  ions,<sup>27,28,31</sup> and the remaining five optical transmittance bands correspond to the  $^3\text{H}_6 \rightarrow ^1\text{G}_4$ ,  $^3\text{F}_{2,3}$ ,  $^3\text{H}_4$ ,  $^3\text{H}_5$ , and  $^3\text{F}_4$  transitions of  $\text{Tm}^{3+}$  ions.<sup>27,28</sup>

To more clearly observe the optical transmittance spectra of  $\text{Er}^{3+}$ ,  $\text{Mn}^{2+}$ , and  $\text{Yb}^{3+}$  ions, we measured and further analyzed the optical transmittance spectra of the SZB-2Mn2Yb, SZB-0.5Er1Tm2Yb, and SZB-0.5Er1Tm2Yb2Mn glass samples. The analyzed results of these optical transmittance spectra are plotted in Fig. 2(B). The obtained results displayed in curve (c)



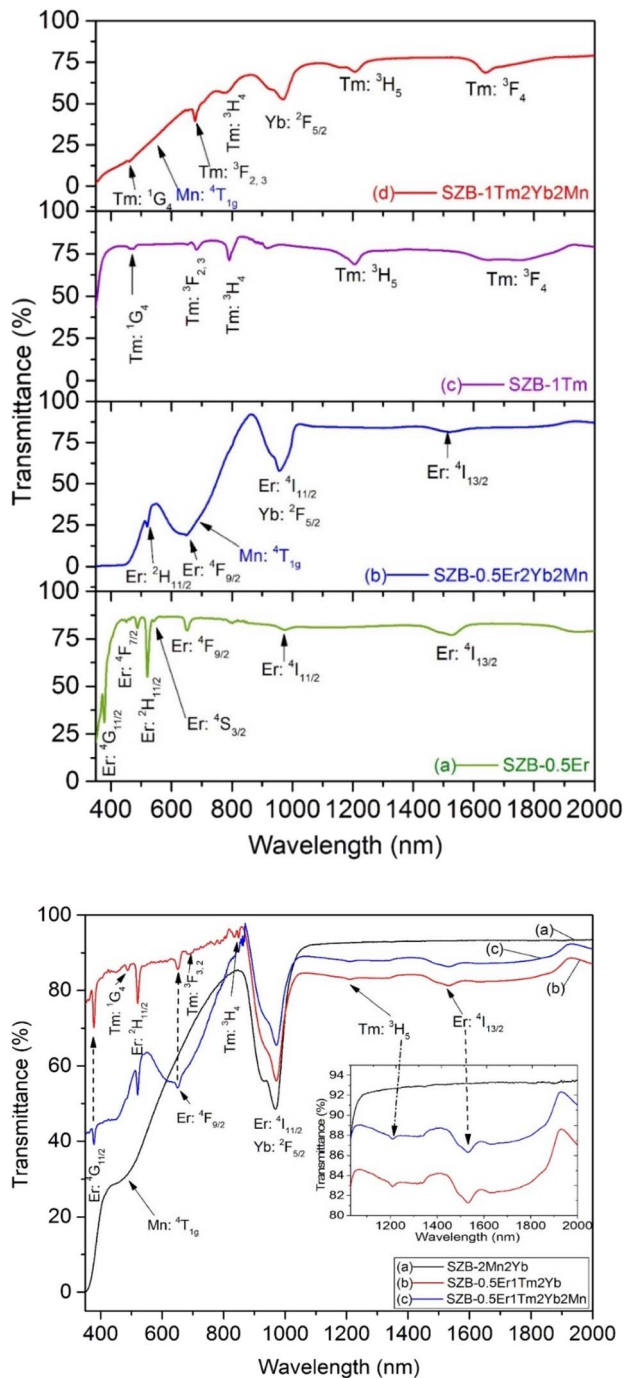


Fig. 2 (A) Optical transmittance spectra of the SZB-0.5Er, SZB-0.5Er2Yb2Mn, SZB-1Tm, and SZB-1Tm2Yb2Mn glass samples. (B) Optical transmittance spectra of the SZB-2Mn2Yb, SZB-0.5Er1Tm2Yb, and SZB-0.5Er1Tm2Yb2Mn glass samples.

of Fig. 2(B) indicate that we can also observe all nine optical transmittance bands corresponding to  ${}^6A_{1g} \rightarrow {}^4T_{1g}$  of  $Mn^{2+}$  ions,  ${}^2F_{7/2} \rightarrow {}^2F_{5/2}$  of  $Yb^{3+}$  ions,  ${}^{4,11,13,14,17}$  and the  ${}^4I_{15/2} \rightarrow {}^4G_{11/2}$ ,  ${}^4F_{7/2}$ ,  ${}^2H_{11/2}$ ,  ${}^4S_{3/2}$ ,  ${}^4F_{9/2}$ ,  ${}^4I_{11/2}$ ,  ${}^4I_{13/2}$  transitions of  $Er^{3+}$  ions,<sup>4,30,31</sup> similar to the analysis above. Interestingly, the analyzed results reveal that the transmittance spectrum of the SZB-0.5Er1Tm2Yb2Mn glass samples containing  $Mn^{2+}$

components in the wavelength region of  $\sim 380$ – $900$  nm was decreased whereas the optical transmittance spectrum in the wavelength region of  $\sim 900$ – $2000$  nm was increased compared to SZB-0.5Er1Tm2Yb glass samples without  $Mn^{2+}$  components. Also from the results displayed in Fig. 2(B), it can be seen that the optical transmittance spectrum of the SZB-2Mn2Yb glass sample within the wavelength range  $\sim 1000$ – $2000$  nm is higher than that of the SZB-0.5Er1Tm2Yb or SZB0.5Er1Tm2Yb2Mn glass samples. For the SZB-0.5Er1Tm2Yb and SZB0.5Er1Tm2Yb2Mn glass samples, in addition to the  $Mn^{2+}$  and  $Yb^{3+}$  components, there are also  $Er^{3+}$  and  $Tm^{3+}$  components with absorption peaks at about 1230 nm and 1542 nm in the wavelength range  $\sim 1000$  to 2000 nm, corresponding to the  ${}^3H_6 \rightarrow {}^3H_5$  transition of  $Tm^{3+}$  ions and the  ${}^4I_{15/2} \rightarrow {}^4I_{13/2}$  transition of  $Er^{3+}$  ions, respectively. Part of the excitation energy is thus absorbed in the wavelength region from  $\sim 1000$  to 2000 nm, which does not occur for the SZB-2Mn2Yb glass sample. This is the reason why the transmittance spectrum of the SZB-2Mn2Yb sample is higher than those of the other glass samples.

### 3.3. NIR emission spectra

NIR emission spectra of the SZB-0.5Er2YbxMn ( $x = 0, 2, 2.5, 3, 3.5$ , and 4 mol%) glass samples under 980 nm LD excitation are plotted in Fig. 3. For the SZB-0.5Er2Yb glass sample, the NIR emission of  $Er^{3+}/Yb^{3+}$ -co-doped peaks at  $\sim 1542$  nm corresponds to the  ${}^4I_{13/2} \rightarrow {}^4I_{15/2}$  transition of  $Er^{3+}$ . With the increased concentrations of the  $MnCO_3$  compound from 2 up to 4 mol%, the NIR emission intensity of the  $Er^{3+}/Yb^{3+}$ -co-doped peaks at  $\sim 1542$  nm was significantly increased. Moreover, the NIR emission peak of  $Er^{3+}$  tends to split and shift the peaks by  $\Delta\lambda = 1553 - 1542$  nm = 11 nm. The main reason for the increase in NIR emission intensity of  $Er^{3+}/Yb^{3+}$ -co-doped peaks at  $\sim 1542$  nm can be attributed to the combination between  $Yb^{3+}$  and  $Mn^{2+}$  ions in the  $MnCO_3$  compound leading to the formation of  $Mn^{2+}-Yb^{3+}$  dimers<sup>13,32</sup> contributing to the energy transfer (ET) to the  ${}^4I_{13/2} \rightarrow {}^4I_{15/2}$  transition of  $Er^{3+}$  ions.<sup>13,23</sup> The

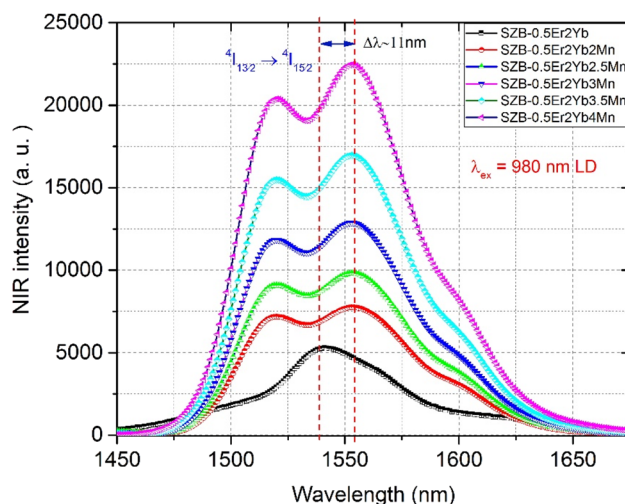


Fig. 3 NIR emission spectra of the SZB-0.5Er2YbxMn ( $x = 0, 2, 2.5, 3, 3.5$ , and 4 mol%) glass samples.

formation of an  $\text{Mn}^{2+}\text{-Yb}^{3+}$  dimer can be interpreted with the result shown in Fig. 3, where the  $\text{Er}^{3+}$  and  $\text{Yb}^{3+}$  concentrations are unchanged when the concentration of the  $\text{MnCO}_3$  compound increases from 2 up to 4 mol%, and the NIR emission intensity of the  $\text{Er}^{3+}/\text{Yb}^{3+}$ -co-doped peaks at  $\sim 1542$  nm under the excitation of 980 nm LD was significantly increased. However, the  $\text{Mn}^{2+}$  ions cannot receive the direct excitation of the 980 nm LD, proving that  $\text{Mn}^{2+}$  ions combine with the  $\text{Yb}^{3+}$  ions to form an  $\text{Mn}^{2+}\text{-Yb}^{3+}$  dimer,<sup>13,23</sup> and therefore, the  $\text{Mn}^{2+}\text{-Yb}^{3+}$  dimers receive the excitation of the 980 nm LD and transfer energy from the  $\text{Mn}^{2+}\text{-Yb}^{3+}$  dimer to the  ${}^4\text{I}_{13/2} \rightarrow {}^4\text{I}_{15/2}$  transition of  $\text{Er}^{3+}$  ions.<sup>13,23</sup> The addition of  $\text{MnCO}_3$  compound into the host glass efficiently promotes not only the formation of the  $\text{Mn}^{2+}\text{-Yb}^{3+}$  dimer but also contributes to breaking of the O-Zn, Si-O, Si-O-Si, Zn-O-Zn, and Si-O-Zn bonds,<sup>33</sup> subsequently creating new non-bridging oxygens (NBOs), like Mn-O, Mn-Si, Si-O-Mn, Mn-O-Mn, and Mn-O-Zn bonds.<sup>34,35</sup> Therefore, we believe that the presence of  $\text{Mn}^{2+}$  ions in the  $\text{MnCO}_3$  compound contributed to shifting the NIR emission peak at the  ${}^4\text{I}_{13/2} \rightarrow {}^4\text{I}_{15/2}$  transition of  $\text{Er}^{3+}$  ions.

We also investigated the effects of  $\text{Mn}^{2+}$  on the NIR emission bandwidth flatness (NIR\_EBF) parameter of  $\text{Er}^{3+}/\text{Yb}^{3+}$  co-doped in SZB glasses. The NIR\_EBF parameter of  $\text{Er}^{3+}/\text{Yb}^{3+}$  co-doped in SZB glasses can be calculated based on the NIR emission spectra of  $\text{Er}^{3+}/\text{Yb}^{3+}$  co-doped in SZB glasses with the following formula:<sup>19,23</sup>

$$\text{NIR\_EBF} = \frac{\sqrt{\prod_{n=0}^{N-1} I(n)}}{\sum_{n=0}^{N-1} I(n)} = \frac{\exp\left(\frac{1}{N} \sum_{n=0}^{N-1} \ln I(n)\right)}{\frac{1}{N} \sum_{n=0}^{N-1} I(n)} \quad (1)$$

where  $I(n)$  is the NIR emission intensity of  $\text{Er}^{3+}/\text{Yb}^{3+}$  co-doped in SZB glasses within the analytical data range  $n$  of the NIR emission wavelength  $N$ .<sup>19,23</sup> NIR\_EBF takes a value from 0 to

1.<sup>19,23</sup> The value of NIR\_EBF is equal to 1 when all values of  $I(n)$  are equal.<sup>19,23</sup> The NIR\_EBF calculated results of  $\text{Er}^{3+}/\text{Yb}^{3+}$  co-doped in SZB glasses displayed in Fig. 4 show that with increasing concentrations of  $\text{Mn}^{2+}$  ions, the NIR\_EBF of  $\text{Er}^{3+}/\text{Yb}^{3+}$  co-doped in SZB glasses gradually decreased.

Similarly, the NIR emission spectra of SZB-1Tm2YbxMn ( $x = 0, 2, 2.5, 3, 3.5,$  and  $4$  mol%) glass samples under excitation of 980 nm LD are plotted in Fig. 5 and indicate that the NIR emission of the  $\text{Tm}^{3+}/\text{Yb}^{3+}$ -co-doped sample has two peaks at about  $\sim 1457$  and  $\sim 1801$  nm, corresponding to the  ${}^3\text{H}_4 \rightarrow {}^3\text{F}_4$  and  ${}^3\text{F}_4 \rightarrow {}^3\text{H}_6$  transitions of  $\text{Tm}^{3+}$  ions.<sup>36,37</sup> Along with the increase in  $\text{MnCO}_3$  concentration from 2 up to 4 mol%, the NIR emission intensity of  $\text{Tm}^{3+}/\text{Yb}^{3+}$ -co-doped peaks at  $\sim 1457$  and  $\sim 1801$  nm was also significantly increased. This result is due to the ET processes from the  $\text{Mn}^{2+}\text{-Yb}^{3+}$  dimer to the  ${}^3\text{H}_4 \rightarrow {}^3\text{F}_4$  and  ${}^3\text{F}_4 \rightarrow {}^3\text{H}_6$  transitions of  $\text{Tm}^{3+}$  ions.<sup>17</sup>

Formula (1) continued to be used to calculate the NIR\_EBF spectra of  $\text{Tm}^{3+}/\text{Yb}^{3+}$ -co-doped samples when the molar concentration of the  $\text{MnCO}_3$  compound increases from 0 up to 4 mol% and the results of the calculation are shown in the insert to Fig. 5. These results show that the NIR\_EBF spectra of the  $\text{Tm}^{3+}/\text{Yb}^{3+}$ -co-doped sample reached the optimal value of 0.668 when the molar concentration of the  $\text{MnCO}_3$  compound was 2 mol%. Energy levels of  $\text{Er}^{3+}$ ,  $\text{Tm}^{3+}$ ,  $\text{Yb}^{3+}$  ions, the  $\text{Mn}^{2+}\text{-Yb}^{3+}$  dimer and mechanisms of the  $\text{ET}_I$  ( $I = 1, 2, 3, 4,$  and  $5$ ) processes in the SZB glass system are shown in Fig. 6. Mechanisms of the  $\text{ET}_I$  ( $I = 1, 2, 3, 4,$  and  $5$ ) processes between the  $\text{Mn}^{2+}\text{-Yb}^{3+}$  dimer with  $\text{Er}^{3+}$ ,  $\text{Tm}^{3+}$  ions were also reported and discussed in detail in our previous studies.<sup>17,26</sup> These  $\text{ET}_I$  ( $I = 1, 2, 3, 4,$  and  $5$ ) processes can be described in detail in the form of the following equations:

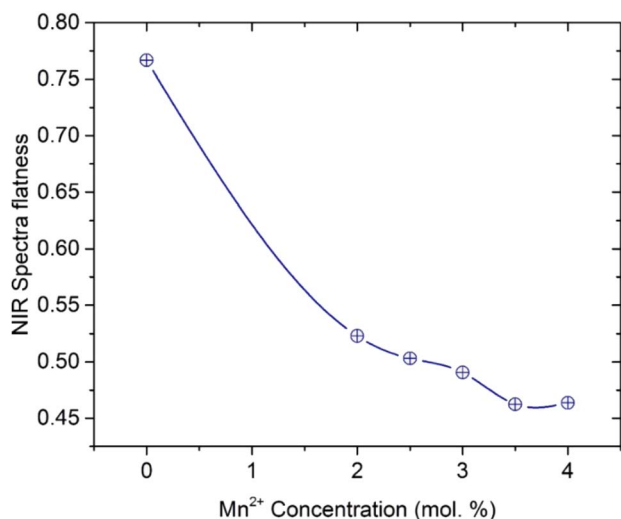
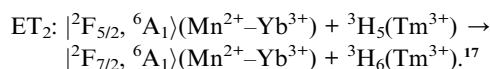
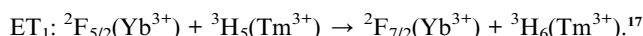


Fig. 4 Relationship between NIR spectra flatness of the SZB-0.5Er2YbxMn ( $x = 0, 2, 2.5, 3, 3.5,$  and  $4$  mol%) glass samples and molar concentration of  $\text{Mn}^{2+}$  ions.

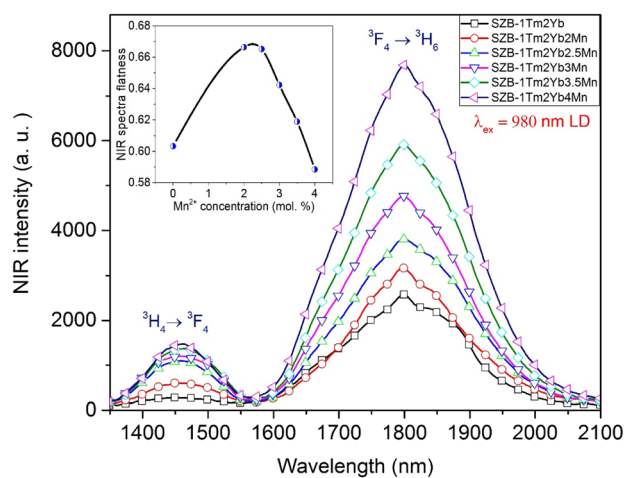


Fig. 5 NIR emission spectra of the SZB-1Tm2YbxMn ( $x = 0, 2, 2.5, 3, 3.5,$  and  $4$  mol%) glass samples.



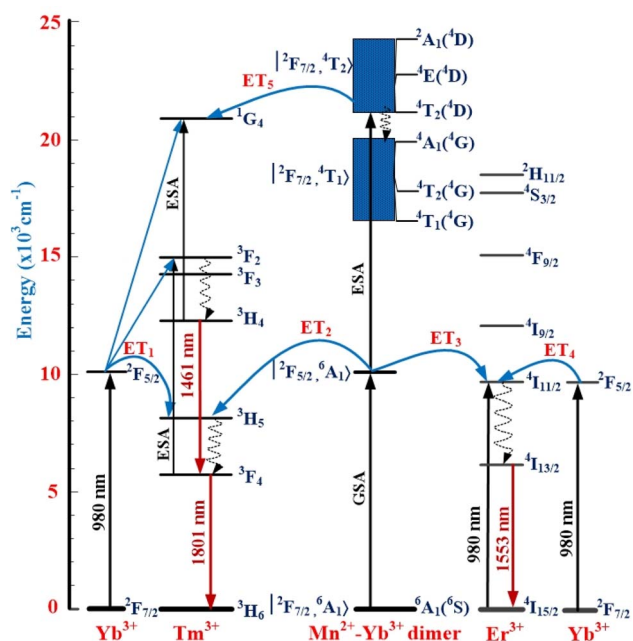
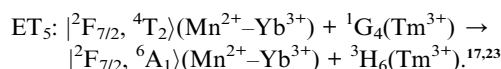
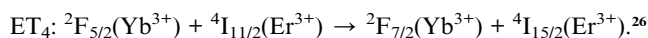
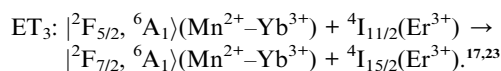


Fig. 6 Energy levels of  $\text{Er}^{3+}$ ,  $\text{Tm}^{3+}$ ,  $\text{Yb}^{3+}$ ,  $\text{Mn}^{2+}$ - $\text{Yb}^{3+}$  dimer and mechanisms of  $\text{ET}_l$  ( $l = 1, 2, 3, 4,$  and  $5$ ) processes in the SZB glass system.



To achieve one of the main goals of this study, we investigated the effects of  $\text{Mn}^{2+}$  ions in the  $\text{MnCO}_3$  compound on the NIR\_EBF spectra of  $\text{Er}^{3+}/\text{Tm}^{3+}/\text{Yb}^{3+}$ -co-doped SZB glasses. We kept the molar compositions of the  $\text{Er}^{3+}/\text{Tm}^{3+}/\text{Yb}^{3+}$ -co-doped

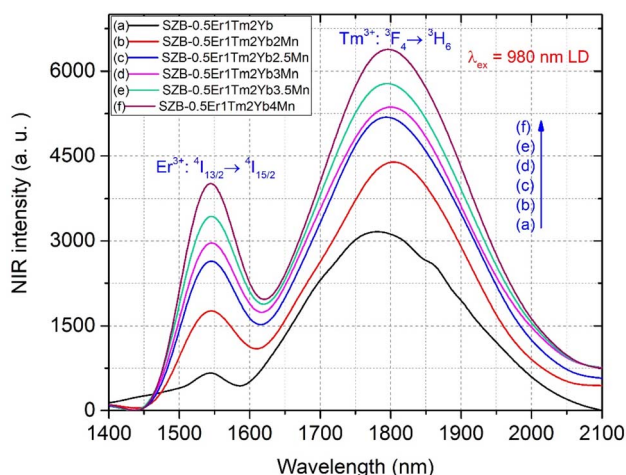


Fig. 7 NIR emission spectra of the SZB-0.5Er1Tm2YbxMn ( $x = 0, 2, 2.5, 3, 3.5,$  and  $4$  mol%) glass samples.

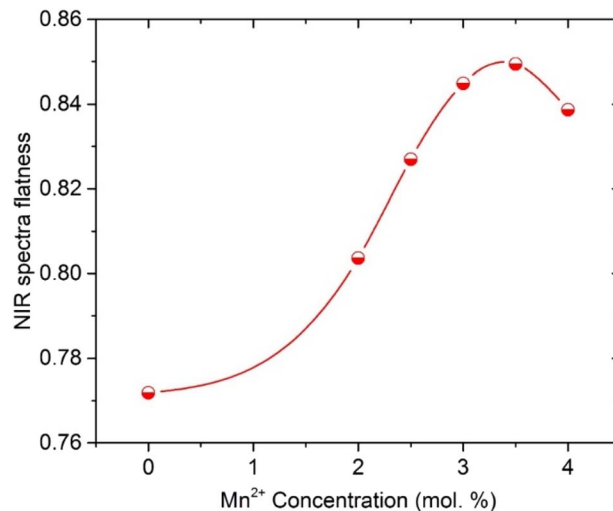


Fig. 8 The relationship between the molar concentration of  $\text{Mn}^{2+}$  ions and NIR\_EBF parameter of the SZB-0.5Er1Tm2YbxMn ( $x = 0, 2, 2.5, 3, 3.5,$  and  $4$  mol%) glass samples.

sample to  $0.5\text{Er}^{3+}/1\text{Tm}^{3+}/2\text{Yb}^{3+}$ , and changed the molar composition of the  $\text{MnCO}_3$  compound from 2 up to 4 mol%. As shown in Fig. 7, the NIR emission spectra of SZB-0.5Er1Tm2YbxMn ( $x = 0, 2, 2.5, 3, 3.5,$  and  $4$  mol%) glass samples under excitation by a 980 nm LD reveal that when the molar concentration of the  $\text{MnCO}_3$  compound increases from 2 up to 4 mol%, the NIR emission intensity of the  $\text{Er}^{3+}/\text{Tm}^{3+}/\text{Yb}^{3+}$ -co-doped peaks at  $\sim 1553$  and  $\sim 1801$  nm also strongly increases. This result may be due to  $\text{Mn}^{2+}$ - $\text{Yb}^{3+}$  dimers being formed during the excitation by 980 nm LD, with the energies from  $\text{Mn}^{2+}$  ions and  $\text{Mn}^{2+}$ - $\text{Yb}^{3+}$  dimers simultaneously transferred to  $\text{Er}^{3+}$  and  $\text{Tm}^{3+}$  ions. The NIR emission spectra of  $\text{Er}^{3+}/\text{Tm}^{3+}/\text{Yb}^{3+}$ -co-doped in the SZB-0.5Er1Tm2YbxMn ( $x = 0, 2, 2.5, 3, 3.5,$  and  $4$  mol%) glass under 980 nm LD excitation created an NIR bandwidth of  $\sim 430$  nm. The NIR\_EBF spectra of the  $\text{Er}^{3+}/\text{Tm}^{3+}/\text{Yb}^{3+}$ -co-doped samples were determined when the molar concentration of  $\text{Mn}^{2+}$  ions in the  $\text{MnCO}_3$  compound increased from 2 up to 4 mol% using formula (1). The results of the calculation of the NIR\_EBF value, given in Fig. 8, showed that the NIR\_EBF spectra of the  $\text{Er}^{3+}/\text{Tm}^{3+}/\text{Yb}^{3+}$ -co-doped sample reached the optimal value of 0.849 when the molar concentration of  $\text{Mn}^{2+}$  ions in the  $\text{MnCO}_3$  compound was 3.5 mol%.

### 3.4. Cross-section and gain coefficient study

To evaluate the influence of  $\text{Mn}^{2+}$  ions in the  $\text{MnCO}_3$  compound on the gain coefficient of  $\text{Er}^{3+}$  ( $G_{\text{Er}}(\lambda)$ ), we first investigated and calculated the absorption cross-section  $\sigma_{\text{abs}}(\lambda)$  and emission cross-section  $\sigma_{\text{ems}}(\lambda)$  for the  ${}^4\text{I}_{13/2} \rightarrow {}^4\text{I}_{15/2}$  transition of  $\text{Er}^{3+}$  ions in the SZB glasses based on McCumber's theory.<sup>6,38,39</sup> The value of  $\sigma_{\text{abs}}(\lambda)$  is calculated from the absorbance spectrum according to the following formula:<sup>6,38,39</sup>

$$\sigma_{\text{abs}}(\lambda) = \frac{2.303}{Cd} A(\lambda), \quad (2)$$

in which  $A(\lambda)$  is the absorbance spectrum;  $\lambda$  is the wavelength;  $C$  is the concentration of  $\text{Er}^{3+}$  ions; and  $d$  is the thickness of the



SZB glass samples, where the glass sample in this study has a thickness of  $d = 2$  mm.<sup>6,38</sup> The absorbance spectrum  $A(\lambda)$  can be calculated from the transmittance spectrum  $T(\lambda)$  according to the formula:<sup>40,41</sup>

$$A(\lambda) = -\log_{10} T(\lambda) = 2 - \log_{10}(\% T(\lambda)), \quad (3)$$

where  $\% T(\lambda)$  is the transmittance spectrum (measured as a percentage) determined from the experimental results in Fig. 2(A) and (B).

The value of  $\sigma_{\text{ems}}(\lambda)$  is thus determined in relation to the value of  $\sigma_{\text{abs}}(\lambda)$  as follows:<sup>6,39</sup>

$$\sigma_{\text{ems}}(\lambda) = \sigma_{\text{abs}}(\lambda) \frac{Z_{\text{L}}}{Z_{\text{U}}} \exp\left(\frac{hc}{kT} \left(\frac{1}{\lambda_{\text{UL}}} - \frac{1}{\lambda}\right)\right), \quad (4)$$

where  $Z_{\text{U}}$  and  $Z_{\text{L}}$  are the partition functions of the upper and lower manifolds, respectively;  $T$  is the temperature;  $h$  is Planck's constant,  $k$  is Boltzmann's constant;  $c$  is the speed of light;  $\lambda$  is the photon wavelength;  $\lambda_{\text{UL}}$  the wavelength corresponding to the transition between the bottom of the excited (upper) state manifold and the bottom of the ground (lower) state manifold.<sup>6,35,36</sup> The value of  $\sigma_{\text{abs}}(\lambda)$  for the  ${}^4\text{I}_{15/2} \rightarrow {}^4\text{I}_{13/2}$  transition and of  $\sigma_{\text{ems}}(\lambda)$  for the  ${}^4\text{I}_{13/2} \rightarrow {}^4\text{I}_{15/2}$  transition of  $\text{Er}^{3+}$  ions are determined as shown in Fig. 9. The gain coefficient  $G(\lambda)$  for transitions of the REIs in the glass samples can be determined with the following formula:<sup>6,38,39</sup>

$$G(\lambda) = C \cdot [P \cdot \sigma_{\text{ems}}(\lambda) - (1 - P) \cdot \sigma_{\text{abs}}(\lambda)], \quad (5)$$

in which  $P$  is the population inversion and  $P = 0-1$  stands for the ratio between the number of REIs in the excited state to the total number of REIs.

Formulae (2)–(5) are used to determine the values of  $\sigma_{\text{abs}}(\lambda)$ ,  $\sigma_{\text{ems}}(\lambda)$ , and  $G_{\text{Er}}(\lambda)$ , respectively, for the  ${}^4\text{I}_{13/2} \rightarrow {}^4\text{I}_{15/2}$  transition of  $\text{Er}^{3+}$  ions in the SZB-0.5Er glass sample. The values of  $G_{\text{Er}}(\lambda)$  were calculated and are shown in Fig. 10. We can observe that the  $G_{\text{Er}}(\lambda)$  value becomes positive in the range wavelength of  $\sim 1500-1600$  nm for cases where  $P$  is equal to 0.5 to 1. When  $P$  is

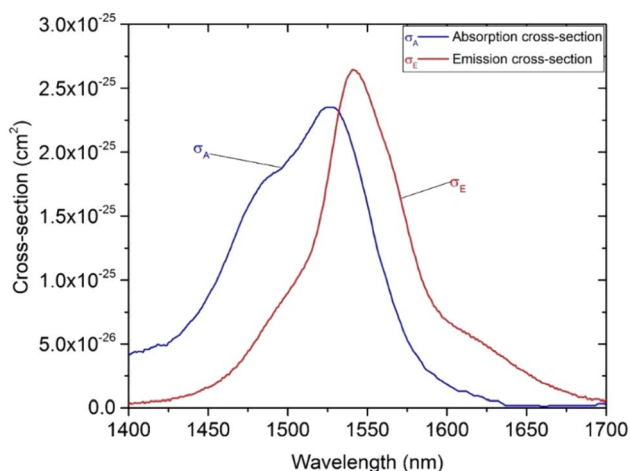


Fig. 9 Absorption and emission cross-sections of the SZB-0.5Er glass sample.

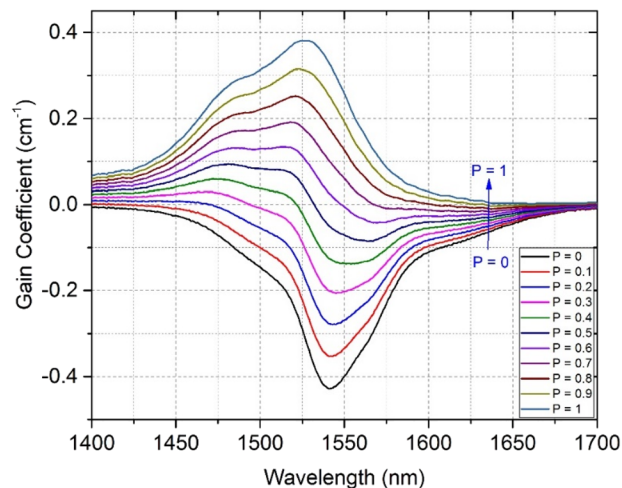


Fig. 10 Gain coefficient for the  ${}^4\text{I}_{13/2} \rightarrow {}^4\text{I}_{15/2}$  transition of  $\text{Er}^{3+}$  ions in the SZB-0.5Er glass sample.

greater than 0.6, the NIR emission of the  $\text{Er}^{3+}$ -doped SZB-0.5Er glass sample exhibits a flat net gain covering the L-, U-, and (L + U)-bands.<sup>6</sup> At the same time, the  $G_{\text{Er}}(\lambda)$  value is found to be about 0.38, corresponding to  $P = 1$ . Similarly, we also used formulae (2)–(5) to determine the values of  $\sigma_{\text{abs}}(\lambda)$ ,  $\sigma_{\text{ems}}(\lambda)$ , and  $G_{\text{Er-Mn}}(\lambda)$ , respectively, for the  ${}^4\text{I}_{13/2} \rightarrow {}^4\text{I}_{15/2}$  transition of  $\text{Er}^{3+}$  ions in the SZB-0.5Er2Yb2Mn glass sample. The values of  $\sigma_{\text{abs}}(\lambda)$  and  $\sigma_{\text{ems}}(\lambda)$  of the SZB-0.5Er2Yb2Mn glass sample are shown in Fig. 11 and the values of  $G_{\text{Er-Mn}}(\lambda)$  for the  ${}^4\text{I}_{13/2} \rightarrow {}^4\text{I}_{15/2}$  transition of  $\text{Er}^{3+}$  ions in the SZB-0.5Er2Yb2Mn glass sample are shown in Fig. 12. Comparison of the results in Fig. 10 and 12 shows that with the existence of  $\text{Mn}^{2+}$  ions in the SZB-0.5Er2Yb2Mn glass sample, the value of  $G_{\text{Er-Mn}}(\lambda)$  for the  ${}^4\text{I}_{13/2} \rightarrow {}^4\text{I}_{15/2}$  transition of  $\text{Er}^{3+}$  ions was significantly reduced. The value of  $G_{\text{Er-Mn}}(\lambda)$  is found to be about 0.21 corresponding to  $P = 1$ . These  $G_{\text{Er-Mn}}(\lambda)$  and  $G_{\text{Er}}(\lambda)$  calculation results showed that in the presence of  $\text{Mn}^{2+}$  ions and an  $\text{Mn}^{2+}\text{-Yb}^{3+}$  dimer, the broadband NIR emission of the  ${}^4\text{I}_{13/2} \rightarrow {}^4\text{I}_{15/2}$  transition of  $\text{Er}^{3+}$

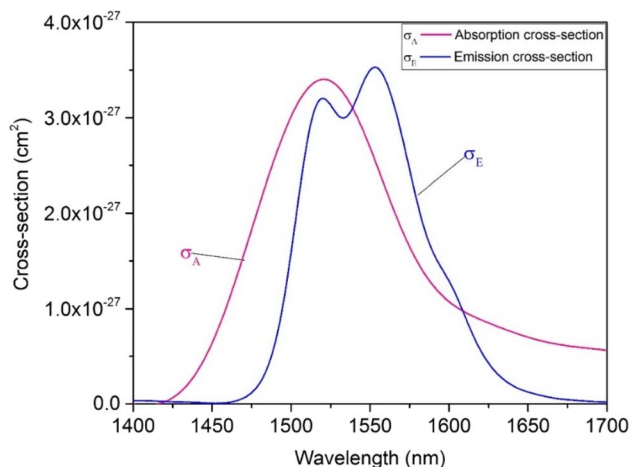


Fig. 11 Absorption and emission cross-sections of the SZB-0.5Er2Yb2Mn glass sample.



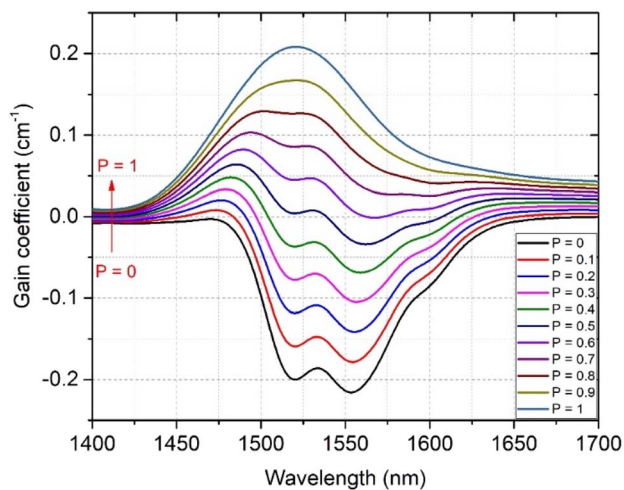


Fig. 12 Gain coefficient for the  ${}^4I_{13/2} \rightarrow {}^4I_{15/2}$  transition of  $\text{Er}^{3+}$  ions in the SZB-0.5Er $_2$ Yb $_2$ Mn glass sample.

ions in this study can be utilized for optical amplifiers. The  $\gamma_G$  ratio between  $G_{\text{Er-Mn}}(\lambda)$  and  $G_{\text{Er}}(\lambda)$  is determined as follows:

$$\gamma_G = \frac{G_{\text{Er-Mn}}(\lambda)}{G_{\text{Er}}(\lambda)} = \frac{0.21}{0.38} = 0.553 \quad (6)$$

Based on the above results and analyses, we can confirm that in the presence of  $\text{Mn}^{2+}$  ions, the NIR bandwidth flatness of  $\text{Er}^{3+}$  ions was improved, but the gain coefficient for the  ${}^4I_{13/2} \rightarrow {}^4I_{15/2}$  transition of  $\text{Er}^{3+}$  ions was significantly reduced. Therefore, depending on the specificity of the application in the optical amplifier, we should choose the type of SZB glass material with or without the  $\text{Mn}^{2+}$  component to suit the specific applications.

## 4. Conclusions

In this work, the effects of  $\text{Mn}^{2+}$  ions in the  $\text{MnCO}_3$  compound leading to the formation of an  $\text{Mn}^{2+}\text{-Yb}^{3+}$  dimer and affecting the gain coefficient for the  ${}^4I_{13/2} \rightarrow {}^4I_{15/2}$  transition of  $\text{Er}^{3+}$  ions and the NIR\_EBF value of  $\text{Er}^{3+}$ -doped and  $\text{Er}^{3+}/\text{Tm}^{3+}/\text{Yb}^{3+}$ -co-doped barium zinc silicate glasses under 980 nm LD excitation were investigated. A broadband NIR emission of  $\text{Er}^{3+}/\text{Tm}^{3+}/\text{Yb}^{3+}$ -co-doped barium zinc silicate glasses with an FWHM of  $\sim 430$  nm was observed. The roles of  $\text{Mn}^{2+}$  ions in the  $\text{MnCO}_3$  compound led to the formation of an  $\text{Mn}^{2+}\text{-Yb}^{3+}$  dimer and contributed to a significant increase in the NIR\_EBF value of  $\text{Er}^{3+}$ -doped and  $\text{Er}^{3+}/\text{Tm}^{3+}/\text{Yb}^{3+}$ -co-doped barium zinc silicate within the NIR wavelength range of 1600–2200 nm. The NIR\_EBF value of  $\text{Er}^{3+}/\text{Tm}^{3+}/\text{Yb}^{3+}$ -co-doped SZB glasses obtained at 0.849 corresponds to the molar concentration of  $\text{MnCO}_3$  compound of 3.5 mol%. However, the presence of  $\text{Mn}^{2+}$  ions in the SZB glass composition also led to a significant decrease in the gain coefficient for the  ${}^4I_{13/2} \rightarrow {}^4I_{15/2}$  transition of  $\text{Er}^{3+}$  ions. The results obtained in this study will be able to guide the selection of glass material compositions for applications in optical amplifiers in the future.

## Conflicts of interest

There are no conflicts of interest to declare.

## Acknowledgements

This research was supported by Project of the TNU-University of Sciences in Vietnam under Grant number CS2023-TN06-10. The corresponding author (Ho Kim Dan) would like to express his gratitude to Van Lang University.

## References

- H. K. Dan, N. M. Ty, V. H. Nga, D. T. Phuc, A.-L. Phan, D. C. Zhou and J. B. Qiu, Broadband flat near-infrared emission and energy transfer of  $\text{Pr}^{3+}\text{-Er}^{3+}\text{-Yb}^{3+}$  tri-doped niobate tellurite glasses, *J. Non-Cryst. Solids*, 2020, **549**, 120335, DOI: [10.1016/j.jnoncrysol.2020.120335](https://doi.org/10.1016/j.jnoncrysol.2020.120335).
- D. C. Zhou, R. F. Wang, Z. W. Yang, Z. G. Song, Z. Y. Yin and J. B. Qiu, Spectroscopic properties of  $\text{Tm}^{3+}$  doped  $\text{TeO}_2\text{-R}_2\text{O-L}_2\text{O}_3$  glasses for 1.47  $\mu\text{m}$  optical amplifiers, *J. Non-Cryst. Solids*, 2011, **357**, 2409–2412, DOI: [10.1016/j.jnoncrysol.2010.12.027](https://doi.org/10.1016/j.jnoncrysol.2010.12.027).
- S. M. Li, L. H. Zhang, X. J. Tan, W. Deng, M. Z. He, G. Z. Chen, M. Xu, Y. L. Yang, S. L. Zhang, P. X. Zhang, Z. Q. Chen and Y. Hang, Growth, structure, and spectroscopic properties of a  $\text{Tm}^{3+}$ ,  $\text{Ho}^{3+}$  co-doped  $\text{Lu}_2\text{O}_3$  crystal for  $\sim 2.1$   $\mu\text{m}$  lasers, *Opt. Mater.*, 2019, **96**, 109277, DOI: [10.1016/j.optmat.2019.109277](https://doi.org/10.1016/j.optmat.2019.109277).
- P. X. Le, N. M. Ty, J. B. Qiu, D. C. Zhou and H. K. Dan, Enhanced upconversion and near-infrared emissions of co-doped  $\text{Ho}^{3+}/\text{Yb}^{3+}$  in  $\text{TeO}_2\text{-ZnO-Na}_2\text{CO}_3\text{-La}_2\text{O}_3$  tellurite glasses, *Opt. Mater. Express*, 2019, **9**, 3998–4008, DOI: [10.1364/OME.9.003998](https://doi.org/10.1364/OME.9.003998).
- X. Wang, X. X. Jin, P. Zhou, X. L. Wang, H. Xiao and Z. J. Liu, High power, widely tunable, narrowband super fluorescent source at 2  $\mu\text{m}$  based on a monolithic Tm-doped fiber amplifier, *Opt. Express*, 2015, **23**(3), 3382–3389, DOI: [10.1364/OE.23.003382](https://doi.org/10.1364/OE.23.003382).
- H. K. Dan, D.-N. Le, H. T. Nguyen-Truong, T. D. Tap, H. X. Vinh, N. M. Ty, R. F. Wang, D. C. Zhou and J. B. Qiu, Effects of  $\text{Y}^{3+}$  the enhancement NIR emission of  $\text{Bi}^{3+}\text{-Er}^{3+}$  co-doped in transparent silicate glass-ceramics for Erbium-doped fiber amplifier (EDFA), *J. Lumin.*, 2020, **219**, 116942, DOI: [10.1016/j.jlumin.2019.116942](https://doi.org/10.1016/j.jlumin.2019.116942).
- P. Peterka, I. Kašík, V. Matějček, W. Blanc, B. Faure, B. Dussardier, G. Monnom and V. Kubeček, Thulium-doped silica-based optical fibers for cladding-pumped fiber amplifiers, *Opt. Mater.*, 2007, **30**, 174–176, DOI: [10.1016/j.optmat.2006.11.039](https://doi.org/10.1016/j.optmat.2006.11.039).
- Y. Guo, J. H. Xie, M. X. Yu, W. T. Huang, H. J. Yang, X. B. Li, L. X. Wang and Q. T. Zhang, The enhanced up-conversion green by Yb-Mn dimer in  $\text{NaBiF}_4$ :  $\text{Yb}^{3+}/\text{Er}^{3+}/\text{Mn}^{2+}$  for optical fiber temperature sensor, *J. Alloys Compd.*, 2021, **888**, 161497, DOI: [10.1016/j.jallcom.2021.161497](https://doi.org/10.1016/j.jallcom.2021.161497).
- L. Z. Xia, Y. Zhang, X. J. Shen and Y. X. Zhou, Broad and flat dual-band NIR luminescence from  $\text{Er}^{3+}/\text{Tm}^{3+}/\text{Ho}^{3+}$  tri-doped



- tellurite glass, *Opt. Lett.*, 2021, **46**(9), 2031–2034, DOI: [10.1364/OL.418971](https://doi.org/10.1364/OL.418971).
- 10 N. Wang, R. J. Cao, M. Z. Cai, L. L. Shen, Y. Tian, F. F. Huang, S. Q. Xu and J. J. Zhang, Ho<sup>3+</sup>/Tm<sup>3+</sup> codoped lead silicate glass for 2 μm laser materials, *Opt. Laser Technol.*, 2017, **97**, 364–369, DOI: [10.1016/j.optlastec.2017.07.025](https://doi.org/10.1016/j.optlastec.2017.07.025).
- 11 S. Ye, Y.-J. Li, D.-C. Yu, G.-P. Dong and Q.-Y. Zhang, Room-temperature upconverted white light from GdMgB<sub>5</sub>O<sub>10</sub>: Yb<sup>3+</sup>, Mn<sup>2+</sup>, *J. Mater. Chem.*, 2011, **21**, 3735–3739, DOI: [10.1039/C0JM03307C](https://doi.org/10.1039/C0JM03307C).
- 12 S. Ye, E. H. Song, E. Ma, S. J. Zhang, J. Wang, X. Y. Chen, Q. Y. Zhang and J. R. Qiu, Broadband Cr<sup>3+</sup>-sensitized upconversion luminescence in La<sub>3</sub>Ga<sub>5</sub>GeO<sub>14</sub>: Cr<sup>3+</sup>, Yb<sup>3+</sup>, Er<sup>3+</sup>, *Opt. Mater. Express*, 2014, **4**(4), 638–648, DOI: [10.1364/OME.4.000638](https://doi.org/10.1364/OME.4.000638).
- 13 H. K. Dan, N. L. Thai, L. D. Tin, J. B. Qiu, D. C. Zhou and Q. Jiao, Enhanced near/mid-infrared emission bands centered at ~1.54 and ~2.73 μm of Er<sup>3+</sup>-doped in transparent silicate glass-ceramics via Mn<sup>2+</sup>–Yb<sup>3+</sup> dimer, *Infrared Phys. Technol.*, 2018, **95**, 33–38, DOI: [10.1016/j.infrared.2018.10.009](https://doi.org/10.1016/j.infrared.2018.10.009).
- 14 J. L. Wang, E. H. Song, M. Wu, W. B. Dai, S. Ye and Q. Y. Zhang, Selectively enhanced up- and down-conversion emissions of Er<sup>3+</sup> via Yb<sup>3+</sup>–Mn<sup>2+</sup> dimer sensitizing in spinel MgGa<sub>2</sub>O<sub>4</sub>: Er<sup>3+</sup>, Yb<sup>3+</sup>, Mn<sup>2+</sup>, *Mater. Res. Bull.*, 2016, **74**, 340–345, DOI: [10.1016/j.materresbull.2015.10.043](https://doi.org/10.1016/j.materresbull.2015.10.043).
- 15 X. X. Han, E. Song, S. Zhang, S. Ye, X. Yang and Q. Zhang, Heavy Mn<sup>2+</sup> doped near-infrared photon upconversion luminescence in Fluoride RbZnF<sub>3</sub>: Yb<sup>3+</sup>, Mn<sup>2+</sup> guided by dopant distribution simulation, *J. Mater. Chem. C*, 2020, **8**, 12164–12172, DOI: [10.1039/D0TC03225E](https://doi.org/10.1039/D0TC03225E).
- 16 C. Pan, Y. Feng-Jing, Z. Zi-Zhong, H. Bo, W. Li-Bo and Z. Ya-Xun, Enhancement of 2.0 μm fluorescence emission in new Ho<sup>3+</sup>/Tm<sup>3+</sup>/Yb<sup>3+</sup> tri-doped tellurite glasses, *Optoelectron. Lett.*, 2016, **12**(5), 0341, DOI: [10.1007/s11801-016-6145-8](https://doi.org/10.1007/s11801-016-6145-8).
- 17 H. K. Dan, D. C. Zhou, R. F. Wang, Q. Jiao, Z. W. Yang, Z. G. Song, X. Yu and J. B. Qiu, Effect of Mn<sup>2+</sup> ions on the enhancement red upconversion emission and energy transfer of Mn<sup>2+</sup>/Tm<sup>3+</sup>/Yb<sup>3+</sup> tri-doped transparent glass-ceramics, *Mater. Res. Bull.*, 2016, **73**, 357–361, DOI: [10.1016/j.materresbull.2015.09.019](https://doi.org/10.1016/j.materresbull.2015.09.019).
- 18 L. Z. Xia, Y. Zhang, X. J. Shen and Y. X. Zhou, Broad and flat dual-band NIR luminescence from Er<sup>3+</sup>/Tm<sup>3+</sup>/Ho<sup>3+</sup> tri-doped tellurite glass, *Opt. Lett.*, 2021, **46**(9), 2031–2034, DOI: [10.1364/OL.418971](https://doi.org/10.1364/OL.418971).
- 19 N. M. Ty, D. C. Zhou, J. B. Qiu and H. K. Dan, Broadband flat near/mid-infrared emissions of Tm<sup>3+</sup>-Ho<sup>3+</sup> co-doped, and Tm<sup>3+</sup>-Ho<sup>3+</sup>-Yb<sup>3+</sup> tri-doped zinc silicate glasses under 808 and 980 nm, *Infrared Phys. Technol.*, 2020, **111**, 103483, DOI: [10.1016/j.infrared.2020.103483](https://doi.org/10.1016/j.infrared.2020.103483).
- 20 N. Shasmal, W. J. G. J. Faria, A. S. Stucchi de Camargo and A. C. M. Rodrigues, Enhancement in green and NIR emissions of Er<sup>3+</sup> by energy transfer from ZnSe nanoparticles in borosilicate glass, *J. Alloys Compd.*, 2021, **863**(15), 158428, DOI: [10.1016/j.jallcom.2020.158428](https://doi.org/10.1016/j.jallcom.2020.158428).
- 21 A. Roy, A. Dwivedi, H. Mishra, A. K. Rai and S. B. Rai, Generation of color tunable emissions from Ho<sup>3+</sup>/Tm<sup>3+</sup>/Yb<sup>3+</sup> co-doped YTaO<sub>4</sub> phosphors through NIR excitation under different conditions (variation of concentration, excitation pump power and the external temperature), *J. Alloys Compd.*, 2021, **865**, 158938, DOI: [10.1016/j.jallcom.2021.158938](https://doi.org/10.1016/j.jallcom.2021.158938).
- 22 M. Kochanowicz, J. Żmojda, P. Miluski, A. Baranowska, T. Ragin, J. Dorosz, M. Kuwik, W. A. Pisarski, J. Pisarska, M. Leśniak and D. Dorosz, 2 μm emission in gallo-germanate glasses and glass fibers co-doped with Yb<sup>3+</sup>/Ho<sup>3+</sup> and Yb<sup>3+</sup>/Tm<sup>3+</sup>/Ho<sup>3+</sup>, *J. Lumin.*, 2019, **211**, 341–346, DOI: [10.1016/j.jlumin.2019.03.060](https://doi.org/10.1016/j.jlumin.2019.03.060).
- 23 H. K. Dan, N. D. Trung, D. C. Zhou and J. B. Qiu, Influences of Mn<sup>2+</sup> ions, and Mn<sup>2+</sup>–Yb<sup>3+</sup> dimer on the optical band gaps and bandwidth flatness of near-infrared emissions of Ho<sup>3+</sup>/Tm<sup>3+</sup>, Ho<sup>3+</sup>/Tm<sup>3+</sup>/Yb<sup>3+</sup> co-doped calcium aluminosilicate glasses, *J. Non-Cryst. Solids*, 2023, **603**, 122086, DOI: [10.1016/j.jnoncrysol.2022.122086](https://doi.org/10.1016/j.jnoncrysol.2022.122086).
- 24 H. Masai, T. Nishibe, S. Yamamoto, T. Niizuma, N. Kitamura, T. Akai, T. Ohkubo and M. Yoshida, Low melting oxide glasses prepared at a melt temperature of 500 °C, *Sci. Rep.*, 2021, **11**, 214, DOI: [10.1038/s41598-020-80424-9](https://doi.org/10.1038/s41598-020-80424-9).
- 25 H. K. Dan, N. D. Trung, T. H. Le, N. L. Thai, N. M. Ty, D. C. Zhou and J. B. Qiu, Influence of F<sup>-</sup> on the reduction process of Eu<sup>3+</sup> to Eu<sup>2+</sup> and optical properties of Eu<sup>3+</sup>/Eu<sup>2+</sup>–Er<sup>3+</sup>–Yb<sup>3+</sup> co-doped niobate silicate glasses, *J. Non-Cryst. Solids*, 2022, **581**, 121417, DOI: [10.1016/j.jnoncrysol.2022.121417](https://doi.org/10.1016/j.jnoncrysol.2022.121417).
- 26 H. K. Dan, D. C. Zhou, R. F. Wang, Q. Jiao, Z. W. Yang, Z. G. Song, X. Yu and J. B. Qiu, Effect of Mn<sup>2+</sup> ions on the enhancement red upconversion emission of Mn<sup>2+</sup>/Er<sup>3+</sup>/Yb<sup>3+</sup> tri-doped in transparent glass-ceramics, *Opt. Laser Technol.*, 2014, **64**, 264–268, DOI: [10.1016/j.optlastec.2014.05.002](https://doi.org/10.1016/j.optlastec.2014.05.002).
- 27 Y. G. Liao, X-ray emission lines & Periodic table for EDS analysis, *Practical electron microscopy and database – An Online Book*, <https://www.globalsino.com/EM>, accessed 15 August, 2023.
- 28 H. K. Dan, N. D. Trung, N. M. Tam, L. T. Ha, C. V. Ha, D. C. Zhou and J. B. Qiu, Optical band gaps and spectroscopy properties of Bi<sup>3+</sup>/Eu<sup>n+</sup>/Yb<sup>3+</sup> co-doped (m = 0, 2, 3; and n = 2, 3) zinc calcium silicate glasses, *RSC Adv.*, 2023, **13**, 6861–6871, DOI: [10.1039/d2ra07310b](https://doi.org/10.1039/d2ra07310b).
- 29 Y. Tsang, B. Richards, D. Binks, J. Lousteau and A. Jha, A Yb<sup>3+</sup>/Tm<sup>3+</sup>/Ho<sup>3+</sup> triply doped tellurite fiber laser, *Opt. Express*, 2008, **16**(14), 10690–10695, DOI: [10.1364/OE.16.010690](https://doi.org/10.1364/OE.16.010690).
- 30 H. K. Dan, N. M. Ty, D. C. Zhou, J. B. Qiu and A.-L. Phan, Influence of Cr<sup>3+</sup> on yellowish-green UC emission and energy transfer of Er<sup>3+</sup>/Cr<sup>3+</sup>/Yb<sup>3+</sup> tri-doped zinc silicate glasses, *J. Am. Ceram. Soc.*, 2020, **103**(11), 1–13, DOI: [10.1111/jace.17359](https://doi.org/10.1111/jace.17359).
- 31 B. T. Huy, D. H. Kwon, S.-S. Lee, V.-D. Dao, H. B. Truong and Y.-I. Lee, Optical properties of Sr<sub>2</sub>YF<sub>7</sub> material doped with Yb<sup>3+</sup>, Er<sup>3+</sup>, and Eu<sup>3+</sup> ions for solar cell application, *J.*



- Alloys Compd.*, 2022, **897**, 163189, DOI: [10.1016/j.jallcom.2021.163189](https://doi.org/10.1016/j.jallcom.2021.163189).
- 32 H. K. Dan, D. C. Zhou, R. F. Wang, Q. Jiao, Z. W. Yang, Z. G. Song, X. Yu and J. B. Qiu, Effect of Mn<sup>2+</sup> ions on the enhancement upconversion emission and energy transfer of Mn<sup>2+</sup>/Tb<sup>3+</sup>/Yb<sup>3+</sup> tri-doped transparent glass-ceramics, *Mater. Lett.*, 2015, **150**, 76–80, DOI: [10.1016/j.matlet.2015.03.005](https://doi.org/10.1016/j.matlet.2015.03.005).
- 33 W. Ahmina, M. E. Moudane, M. Zriouil and M. Taibi, Glass-forming region, structure and some properties of potassium manganese phosphate glasses, *Phase Transform.*, 2016, **89**, 1051–1061, DOI: [10.1080/01411594.2016.1144057](https://doi.org/10.1080/01411594.2016.1144057).
- 34 J. de Clermont-Gallerande, D. Taniguchi, M. Colas, P. Thomas and T. Hayakawa, High-temperature investigation of TeO<sub>2</sub>–Na<sub>2</sub>O–ZnO glasses, *Phys. Status Solidi B*, 2022, **259**, 2200065, DOI: [10.1002/pssb.202200065](https://doi.org/10.1002/pssb.202200065).
- 35 P. Pascuta, G. Borodi, N. Jumate, I. Vida-Simiti, D. Viorel and E. Cule, The structural role of manganese ions in some zinc phosphate glasses and glass ceramics, *J. Alloys Compd.*, 2010, **504**, 479–483, DOI: [10.1016/j.jallcom.2010.05.147](https://doi.org/10.1016/j.jallcom.2010.05.147).
- 36 G. Bai, Y. Guo, Y. Tian, L. Hu and J. Zhang, Light emission at 2 μm from Ho–Tm–Yb doped silicate glasses, *Opt. Mater.*, 2011, **33**(8), 1316–1319, DOI: [10.1016/j.optmat.2011.03.033](https://doi.org/10.1016/j.optmat.2011.03.033).
- 37 C. Z. Wang, Y. Tian, X. Y. Gao, Q. H. Liu, F. F. Huang, B. P. Li, J. J. Zhang and S. Q. Xu, Mid-infrared fluorescence properties, structure and energy transfer around 2 μm in Tm<sup>3+</sup>/Ho<sup>3+</sup> co-doped tellurite glass, *J. Lumin.*, 2018, **194**, 791–796, DOI: [10.1016/j.jlumin.2017.09.052](https://doi.org/10.1016/j.jlumin.2017.09.052).
- 38 G. Y. Zhao, L. Z. Xu, S. H. Meng, C. B. Du, J. S. Hou, Y. F. Liu, Y. Y. Guo, Y. Z. Fang, M. S. Liao, J. Zou and L. L. Hu, Facile preparation of plasmon enhanced near-infrared photoluminescence of Er<sup>3+</sup>-doped Bi<sub>2</sub>O<sub>3</sub>–B<sub>2</sub>O<sub>3</sub>–SiO<sub>2</sub> glass for optical fiber amplifier, *J. Lumin.*, 2019, **206**, 164–168, DOI: [10.1016/j.jlumin.2018.10.026](https://doi.org/10.1016/j.jlumin.2018.10.026).
- 39 Z. Y. Zhao, C. Liu, M. L. Xia, J. Wang, J. J. Han, J. Xie and X. J. Zhao, Effects of Y<sup>3+</sup>/Er<sup>3+</sup> ratio on the 2.7 μm emission of Er<sup>3+</sup> ions in oxyfluoride glass-ceramics, *Opt. Mater.*, 2016, **54**, 89–93, DOI: [10.1016/j.optmat.2016.02.022](https://doi.org/10.1016/j.optmat.2016.02.022).
- 40 T. G. Mayerhöfer, S. Pahlow and J. Popp, The Bouguer-Beer-Lambert Law: Shining light on the obscure, *ChemPhysChem*, 2020, **21**, 2029–2046, DOI: [10.1002/cphc.202000464](https://doi.org/10.1002/cphc.202000464).
- 41 N. Ilie, A. C. Ionescu, K. C. Huth and M. Moldovan, Light transmission characteristics and cytotoxicity within a dental composite color palette, *Materials*, 2023, **16**, 3773, DOI: [10.3390/ma16103773](https://doi.org/10.3390/ma16103773).

